Atmos. Chem. Phys. Discuss., 11, 17789–17823, 2011
www.atmos-chem-phys-discuss.net/11/17789/2011/
doi:10.5194/acpd-11-17789-2011

Atmospheric Chemistry and Physics Discussions

Accounting for non-linear chemistry of ship plumes in the GEOS-Chem global chemistry transport model

G. C. M. Vinken[1,*], **K. F. Boersma**[1,2], **D. J. Jacob**[3], **and E. W. Meijer**[4]

[1]Eindhoven University of Technology, Eindhoven, The Netherlands
[2]Royal Netherlands Meteorological Institute, De Bilt, The Netherlands
[3]Harvard University, Cambridge, USA
[4]TNO, Utrecht, The Netherlands

[*] *Invited contribution by G. C. M. Vinken, recipient of the EGU Outstanding Student Poster Award 2011.*

Received: 27 May 2011 – Accepted: 13 June 2011 – Published: 23 June 2011

Correspondence to: G. C. M. Vinken (g.c.m.vinken@tue.nl)

Published by Copernicus Publications on behalf of the European Geosciences Union.

Abstract

We present a computationally efficient approach to account for the non-linear chemistry occurring during the dispersion of ship exhaust plumes in a global 3-D model of atmospheric chemistry (GEOS-Chem). We use a plume-in-grid formulation where ship emissions age chemically for 5 h before being released in the global model grid. Besides reducing the original ship NO_x emissions in GEOS-Chem, our approach also releases the secondary compounds ozone and HNO_3, produced in the 5 h after the original emissions, into the model. We applied our improved method and also the widely used "instant dilution" approach to a 1-yr GEOS-Chem simulation of global tropospheric ozone-NO_x-VOC-aerosol chemistry. We also ran simulations with the standard model, and a model without any ship emissions at all. Our improved GEOS-Chem model simulates up to 0.1 ppbv (or 90 %) more NO_x over the North Atlantic in July than GEOS-Chem versions without any ship NO_x emissions at all. "Instant dilution" overestimates NO_x concentrations by 50 % (0.1 ppbv) and ozone by 10–25 % (3–5 ppbv) over this region. These conclusions are supported by comparing simulated and observed NO_x and ozone concentrations in the lower troposphere over the Pacific Ocean. The comparisons show that the improved GEOS-Chem model simulates NO_x concentrations in between the instant diluting model and the model with no ship emissions, and results in lower O_3 concentrations than the instant diluting model. The relative differences in simulated NO_x and ozone between our improved approach and instant dilution are smallest over strongly polluted seas (e.g. North Sea), suggesting that accounting for in-plume chemistry is most relevant for pristine marine areas.

1 Introduction

Seagoing ships carry approximately 90 % of the goods traded globally and the seaborne trade has been estimated to increase by 5 % per year between 2002 and 2007 (Eyring et al., 2010). These ships emit large quantities of gases and particles into the marine boundary layer. Important gas-phase products of fuel combustion from

ACPD
11, 17789–17823, 2011

shipping are nitrogen oxides ($NO_x = NO + NO_2$). NO_x emissions lead to photochemical production of ozone (O_3) and influence the hydroxyl-radical (OH) concentrations that determine the lifetime of methane (CH_4) (Lawrence and Crutzen, 1999), both significant contributors to global radiative forcing (IPCC, 2007). Furthermore, high O_3 mixing ratios in the lower troposphere are a key component of photochemical smog and pose a threat to human health and vegetation. 70 % of ship emissions are estimated to occur within 400 km of land (Corbett et al., 1999), so ships contribute significantly to pollution in highly populated coastal areas.

Ships are strong polluters because they are still allowed to combust marine heavy fuel. Marine engines combust this fuel at high temperatures, leading to relatively high NO_x emissions. No international legislative framework is currently in place for monitoring and allocating international ship emissions. Only recently, the European Union and the United States Environmental Protection Agency (EPA) issued the mandatory use of cleaner shipping fuel types in the increasingly polluted harbor regions. Previous studies (e.g. Corbett et al., 2007; Eyring et al., 2010) indicate that the total NO_x emissions of shipping are in the range 3.0–10.4 Tg N per year, amounting to 15–30 % of total global NO_x emissions.

State-of-science knowledge of the impact of ship emissions relies on emissions inventories in combination with model studies (e.g. Corbett et al., 1999; Eyring et al., 2005; Wang et al., 2008; Marmer et al., 2009). Standard Eulerian chemistry-transport models (CTMs) simulate atmospheric concentrations of air pollutants by instant dilution of highly localized sources (e.g. power plants, highways) over the entire model grid cell. This is an acceptable simplification for chemically inert species, and probably also for chemically reactive species, provided that there are many such sources within a model cell. However, when emitting chemically reactive species from highly localized sources in relatively clean areas (e.g. ship stacks), instant dilution leads to unrealistically high NO_x and O_3 concentrations (Davis et al., 2001). Such overestimations occur because non-linear chemistry during the initial dispersion stage of the plume is neglected in the instant dilution approach. For example, Kasibhatla et al. (2000) found

ACPD
11, 17789–17823, 2011

that their instantly diluting (GFDL, 5° × 5°) model simulated NO_x concentrations that were 10× higher than observations over the central North Atlantic. Franke et al. (2008) reported that instant dilution of ship NO_x emissions in a grid box comparable to the grid cell size of a global model (2.8° × 2.8°), leads to overestimation of ship-induced ozone production by a factor three. A recent study by Charlton-Perez et al. (2009) suggests, by comparing simulations at different resolutions from a high resolution CTM (200 m × 200 m × 40 m), that a coarse-grid CTM (5° × 5°) might overestimate O_3 production by a factor 1.6. Several studies with Lagrangian models (e.g. von Glasow et al., 2003; Song et al., 2003; Chen et al., 2005) showed that the NO_x lifetime within ship plumes is a factor 2.5–10 shorter than the lifetime of roughly 1 day estimated by the instantly diluting CTMs. These Lagrangian models account for the higher NO_x concentrations in the initial dispersion stages of the plume, leading to elevated OH levels and thereby shorter NO_x lifetimes.

Not a single global CTM currently takes the in-plume effects during ship plume dispersion into account. Most models use instant dilution to mix ship emissions with background concentrations of trace gases. The GEOS-Chem model (Bey et al., 2001) attempts to avoid model errors associated with instant dilution, by replacing every emitted NO_x molecule by 10 O_3 and 1 HNO_3 molecules, based on the average ozone production efficiency of 10 (O_3 molecules produced per NO_x molecule consumed) observed over the eastern Pacific Ocean near California (Chen et al., 2005). Although this approach appears to overcome some of the model errors encountered by other CTMs, it erroneously produces O_3 at night, neglects effects of temperature and ambient concentrations on O_3-NO_x chemistry, and underestimates NO_x concentrations in shipping routes, making it practically impossible to use the model in combination with in situ or satellite observations of NO_x to constrain ship NO_x emissions. The Global Modeling Initiative's (GMI) tropospheric CTM used by Duncan et al. (2008) corrects for the continuous O_3 production at night by scaling the ozone production efficiency with the NO_2 photolysis rate, but does not account for the effects of temperature and ambient concentrations either.

ACPD
11, 17789–17823, 2011

One way to accurately represent highly localized emissions in remote locations in coarse global models, is by using the concept of "effective emissions". In this approach, a small-scale model is used to evaluate the effects of non-linear chemistry on the enhanced concentrations in a plume up until the moment that sub-grid chemical nonlinearities have sufficiently decayed, and subsequently introduce the emissions as (reduced) "effective emissions" in the large-scale model (in the past used for dealing with urban and power plant plume in Eulerian models, Sillman et al., 1990). Such an approach has been attempted for aircraft emissions in the TM3 global CTM (Meijer et al., 1997) and recently also for ship emissions in a regional model (Huszar et al., 2010). Huszar et al. (2010) found, using a regional CTM (CAMx) over Europe, that the large scale NO_x concentrations decrease and the ship NO_x contribution is reduced by up to 20–25 % (compared to instant dilution) and that the ship induced ozone production was reduced by 15–30 % over large areas of Europe.

In this study we propose a method to accurately implement ship emissions using plume-in-grid approach, accounting for non-linear chemistry during the early stages of plume dispersion, in the GEOS-Chem global CTM. We model the effects of non-linear chemistry within a ship exhaust plume with a Gaussian dispersion model that includes complete atmospheric chemistry. In situ observations of trace gases in ship plumes are used to test our Gaussian dispersion model. We test and evaluate various approaches of dealing with ship emissions in a global CTM with observations over the Atlantic and Pacific Ocean.

2 Model

2.1 PARANOX model

In this study a Gaussian dispersion plume model, named PARANOX (PARAmetrization of emitted NOX) has been used. The basic characteristics of this model were described by Meijer (2001) and Vinken (2010). This model was originally designed to simulate

ACPD
11, 17789–17823, 2011

the effects of aircraft emissions in the upper troposphere, but for this study we adapted it to marine boundary layer conditions. The model simulates the chemical evolution of atmospheric trace gas concentrations resulting from emissions in 10 rings perpendicular to the wind direction, as a cross-section of the plume. The model takes into account the chemistry inside and outside the plume, diffusion of emitted species inside the plume between the rings, expansion of the plume, and entrainment of ambient air in the plume. In this section we first describe the general characteristics of PARANOX and then evaluate PARANOX with ship plume observations from the ITCT 2K2 aircraft campaign (Chen et al., 2005).

The model includes a detailed simulation of O_3-NO_x-hydrocarbon chemistry for the troposphere, with 43 species and 98 reactions. Originally the gas-phase reaction rates were taken from DeMore et al. (1997). We updated PARANOX with the latest reaction rates from the IUPAC Subcommittee for Gas Kinetic Data Evaluation (http://www.iupac-kinetic.ch.cam.ac.uk/index.html). Rainout of species is not taken into account. The time step in the model is 100 s. To facilitate the discussion of plume chemistry in the remainder of the paper, the most critical O_3-NO_y-HO_x reactions for both day and nighttime are given in Table 1.

Sulfate particles are formed in the ship plume, that allow heterogeneous reactions in the plume. The PARANOX model includes heterogeneous formation of HNO_3 from N_2O_5 and H_2O on aerosols. The reaction rate constant K_{het} (s^{-1}) of Reaction (R12) is given by

$$K_{het} = \frac{1}{4}\gamma v S \quad (1)$$

With γ the reaction probability, S (cm^{-1}) the aerosol surface area density, and v ($cm\,s^{-1}$) the mean absolute molecular velocity of air molecules. Originally the reaction probability of N_2O_5 on sulphate aerosol was 0.1 as suggested for tropospheric conditions above 200 K by DeMore et al. (1997). Following recent studies, e.g. Evans and Jacob (2005), we updated this reaction probability to 0.02.

ACPD
11, 17789–17823, 2011

In this study we follow an approach for the lateral and vertical dispersion in the lower troposphere originally described by Hanna et al. (1985) (Offshore and Coastal Dispersion algorithm), adapted for dispersion calculations over water by Song et al. (2003) and commonly used to describe ship plume dispersion (e.g. Franke et al., 2008; Kim et al., 2009; Song et al., 2010). These lateral and vertical dispersion parameters depend on the meteorological stability class and can be tuned in PARANOX. The marine boundary layer is often topped by an inversion. It is generally assumed that plumes will not expand above this top. Therefore, we stop expansion in the vertical direction when the outer radius of the 10th ring reaches this top. After this top has been reached the expansion in the lateral direction still continues.

2.2 Evaluation of PARANOX

In order to validate the simulations by the plume model we compare our results with observations from the ITCT 2k2 aircraft campaign (Chen et al., 2005). In this study, measurements were taken from a ship plume 100 km off the Californian coast around noon on 8 May 2002. Measurements of chemical species concentrations were taken from the aircraft at ~100 m above sea level in eight consecutive transects of the ship plumes, corresponding to plume ages of 30 min up to 3 h. Concentrations of NO_x, HNO_3, PAN, SO_2, H_2SO_4, O_3, CO and CO_2 have been measured.

For the PARANOX evaluation we used a NO_x emissions rate of 12.4 g s^{-1}, as reported for the ITCT 2K2 aircraft campaign by (Chen et al., 2005). We adopt background concentrations as given in Table 2, consistent with the values reported for the ITCT 2K2 aircraft campaign.

Figure 1 shows the evolution of observed and simulated NO_x, O_3 and OH concentrations, as well as the instantaneous NO_x lifetime, in the plume in the 3 h after emissions. The PARANOX simulated concentrations correspond to the weighted average over the 10 rings.

To structure the discussion of the results we separate the plume dispersion in three regimes, as proposed by Song et al. (2003): early plume dispersion ([NO_x] above

ACPD
11, 17789–17823, 2011

1 ppmv), mid-range dispersion ([NO_x] ~ several ppbv) and long-range dispersion ([NO_x] below 1 ppbv). We can also classify the evolution of the plume by following the O_3 concentrations: O_3 titration ([O_3] less than half of ambient concentration), O_3 recovery ([O_3] increasing to ambient concentration) and net O_3 production ([O_3] above ambient concentration).

The strong decline in the O_3 concentrations during the first stage is caused by the O_3 being titrated by the abundantly available NO via Reaction (R3). Almost all O_3 within the plume is gone at this point, but stored as NO_2 and will later be recycled. In the second stage, HO_2 is converted to OH and NO_2 via Reaction (R4) (this is reflected by the rise in OH concentrations in Fig. 1c). The NO_2 is then photolyzed (Reaction R5), leading to net photochemical O_3 production (Fig. 1b). The OH concentrations are maximal in this stage and almost 2 times higher than background levels. These high OH concentrations imply a shorter NO_x lifetime and a relatively low fraction of NO_x remaining. By instantly diluting the emissions, common practice in global CTMs, this stage is missing and this results in too high NO_x lifetimes. After about 80 min the final stage sets in. Reactions of NO with HO_2 (Reaction R4) and organic peroxides (e.g. CH_3O_2, Reaction R9), lead to increasing levels of photochemically produced O_3, as shown in Fig. 1b. All three stages show that PARANOX simulations agree with the observed concentrations.

As mentioned before, the main problem in global CTMs is the overestimation of the lifetime of ship emitted NO_x due to instant dilution. In this study we define the NO_x lifetime within the plume in terms of how fast NO_x is lost at a given point in time, the so-called "instantaneous lifetime":

$$\tau_{NO_x} = \frac{[NO] + [NO_2]}{P_{HNO_3}} \quad (2)$$

The main sink of NO_x during the day is reaction of NO_2 with OH via Reaction (R2), i.e. the production of HNO_3. At night it is mainly controlled by Reactions (R6) and (R7), which involve the formation of NO_3 and N_2O_5, followed by HNO_3 formation from N_2O_5 on sulfate aerosols (Reaction R12).

ACPD
11, 17789–17823, 2011

Figure 1d shows that both the observed and simulated NO_x lifetime in the plume is lower than the background lifetime. We conclude that the PARANOX model is able to capture the non-linear chemistry occurring in a dispersive ship plume, and we will now use it to account for these effects in the global CTM GEOS-Chem.

3 Using PARANOX to account for non-linear plume chemistry

As running PARANOX online for every ship plume would be computationally too expensive, the PARANOX model is used to calculate look-up tables (LUTs) to account for the non-linear chemistry in a dispersive ship plume in the global CTM. First, we perform a sensitivity analysis to determine the critical (environmental) parameters that need to be included in the LUT. Once the most critical dependencies are known, we can calculate LUTs for the fraction of NO_x remaining and integrated net ozone production efficiency (NOPE). In these LUTs we save the fraction of NO_x remaining and the integrated NOPE as a function of critical environmental parameters at the end of the PARANOX simulation, that we set at 5 h (see discussion in Sect. 3.3). Values for the environmental parameters are taken from GEOS-Chem simulations at the location and time of the ship emissions.

3.1 Fraction of NO_x remaining and integrated NOPE

We apply PARANOX to simulate the in-plume effects for various environmental conditions, and calculate the fraction of NO_x remaining and the integrated NOPE. The fraction of NO_x remaining is determined by dividing the mass of the emitted NO_x, chemically evolved to NO, NO_2, NO_3, N_2O_5, HONO, HO2NO2 or PAN (excluding HNO_3), in the plume at time t by the mass of emitted NO_x in the plume at time $t = 0$. The fraction of NO_x remaining will be used to reduce the amount of NO_x upon release at time t in the global CTM with the coarse spatial resolution.

ACPD
11, 17789–17823, 2011

An important concept in O_3 production by NO_x emissions is the Net Ozone Production Efficiency (NOPE). The NOPE (ω) is defined as the cross-plume integral of net number of ozone molecules produced divided by the cross-plume integral of ship emitted NO_x consumed at any point in time. In PARANOX, we label the emitted NO_x molecules, so that we can distinguish between O_3 molecules produced (or lost) from ship NO_x and O_3 molecules produced from in-plume entrainment of ambient NO_x. In this study we take the loss of NO_x to be equal to the production of HNO_3, leading to

$$\omega = \frac{P_{O_3} - L_{O_3}}{P_{HNO_3}} \tag{3}$$

HNO_3 is the main sink for NO_x and is removed by deposition. PARANOX does not take deposition into account, but the global CTM eventually solves removal by deposition, as we will see in Sect. 4.

The NOPE described above should be regarded as an "instantaneous NOPE". When using the ship plume model as a pre-processor to calculate effective ship emissions we need to assess the NOPE during the entire plume expansion. For this reason we introduce the "integrated NOPE". This integrated NOPE (Ω) is determined by the ratio of the total net ozone produced (by the ship emitted NO_x) and the total (ship emitted) NO_x lost (HNO_3 produced), averaged over all rings, between $t' = 0$ and t:

$$\Omega = \frac{\int_{t'=0}^{t} \{P_{O_3} - L_{O_3}\} dt'}{\int_{t'=0}^{t} P_{HNO_3} dt'} \tag{4}$$

in which t is the end time of the model (order of several hours).

3.2 Sensitivity analysis

The fraction of NO_x remaining and the integrated NOPE depend on atmospheric composition and meteorological conditions. Before calculating the fraction of NO_x

ACPD
11, 17789–17823, 2011

remaining and integrated NOPE for our look-up tables, we identified the dependencies that have the strongest influence.

Figure 2 shows the fraction of NO_x remaining after 5 h as a function of the most important environmental parameters for an initial release at 12:00 h local time. Higher temperatures lead to lower fractions of NO_x remaining, as shown in Fig. 2a. Figure 2b shows that the fraction of NO_x remaining decreases with O_3 concentrations, because these favor OH formation (via Reaction R1), that in turn lowers the NO_x lifetime. For increasing ambient NO_x concentrations, the fraction of (ship) NO_x remaining initially decreases (Fig. 2c). For ambient concentrations above 1–2 ppbv, the fraction of NO_x remaining increases, as O_3 is titrated and OH concentrations decrease. In Fig. 2d it is shown that higher values of $J(NO_2)$ lead to lower fractions of NO_x remaining. Higher values of $J(NO_2)$ represent more sunlight and a more photochemically active regime, leading to lower NO_x lifetimes. Figure 2e shows that the fraction of NO_x remaining decreases with $\frac{J(O(^1D))}{J(NO_2)}$, reflecting an increase in OH produced via Reaction (R1). The solar zenith angle at the time of emission (θ_0) is an important parameter in determining the fraction of NO_x remaining, as illustrated by Fig. 2f. For a value of $\theta_0 = 10^\circ$ (noon at low latitudes), the plume started expanding at a time when the sun was high, and photolysis was strong, leading to a short instantaneous NO_x lifetime, as reflected by the low fraction of NO_x remaining. The apparent jump in the fraction of NO_x remaining at $\theta_0 = 90^\circ$ marks the difference between a plume that expanded in darkness and a plume that expanded in sunlight for 5 h. Figure 2g shows that the fraction of NO_x remaining also depends on the solar zenith angle 5 h after release, and the effect is similar to the sensitivity to θ_0.

Figure 3 shows the integrated NOPE after 5 h as a function of the most important environmental parameters for an initial release at 12:00 p.m. Figure 3a shows the sensitivity of the integrated NOPE to temperature, and can be explained by the subsequent changes in H_2O concentrations. The integrated NOPE decreases strongly with increasing background O_3 concentrations, as is shown in Fig. 3b. Additional simulations show that this is due to a combination of lower O_3 production, higher O_3 loss and

ACPD
11, 17789–17823, 2011

increased NO_x loss as in Fig. 2b. Figure 3c indicates that for higher NO_x concentrations, O_3 production becomes less efficient. When ambient NO_x concentrations exceed 2 ppbv, O_3 loss (via titration) exceeds O_3 production and the NOPE may become negative. In Fig. 3d, we see that the integrated NOPE increases as a function of $J(NO_2)$, as high values of $J(NO_2)$ increase photochemical ozone production via Reaction (R5). The NOPE decreases for increasing $\frac{J(O(^1D))}{J(NO_2)}$ ratios, reflecting enhanced photolysis loss through Reaction (R1), as illustrated by Fig. 3e. As expected, the solar zenith angles are important parameters for the integrated NOPE. For example, Fig. 3f, $\theta_0 = 10^\circ$ implies a strong integrated NOPE. In contrast, when the plume expansion started at night ($\theta_0 > 90$), the integrated NOPE is negative, reflecting O_3 loss. The sensitivity of the integrated NOPE to the solar zenith angle 5 h after release (θ_5) differs more from that of θ_0 than for the fraction of NO_x remaining. If the plume was in daylight at the end of the 5 h, the NO_x concentrations are lower due to expansion and the plume is more efficient at producing ozone, hence this leads to a higher integrated NOPE, as can be seen by comparing Fig. 3f and g.

3.3 Look-up table

We proceed and calculate two look-up tables (LUTs), storing the fraction of NO_x remaining and the integrated NOPE as a function of 7 parameters after 5 h: temperature, $J(NO_2)$, $\frac{J(O(^1D))}{J(NO_2)}$, (ambient) O_3 concentrations, (ambient) NO_x concentrations and the solar zenith angles at $t = 0$ and $t = -5$ h. These parameters were identified by the sensitivity analysis and Figs. 2 and 3.

Our sensitivity analysis pointed out that the combination of low wind speed, lowmarine boundary layer height, and high emissions is important in causing a saturation effect. This effect causes the fraction of NO_x to increase with decreasing wind speeds, with decreasing marine boundary layer heights and with increasing emissions. If such situations occur frequently in GEOS-Chem it would be important to include these parameters in the LUT. In this study we adopt a relative modest NO_x emission strength

ACPD
11, 17789–17823, 2011

of 20 g s^{-1}, in line with most estimates. Table 3 shows the current estimates used in literature. The fluxes at the high end of the distribution, reported by Franke et al. (2008) and Schlager et al. (2008), hold for "fairly large container ships", which is unlikely to represent the global fleet average emission strength. Furthermore we analyzed the ensemble of GEOS-Chem simulations and concluded that low wind speed events combined with a low MBL occur infrequently (less than 4 %). This led us – in combination with modest NO_x emission strength of 20 g s^{-1} – to decide to not include wind speed and MBL in the LUT.

The run time of PARANOX is an important parameter in the PARANOX model. Choosing it too short might lead to a too high fraction of NO_x remaining and thus too much ozone production when diluted back into the global model. Choosing it too long exposes our simulations to transport of the plume-in-grid outside of the grid cell, especially for situations with strong winds. Another parameter influenced by the run time is the size of the plume. We chose 5 h in our runs as this will also allow the plumes to be well dispersed for higher mixing depths and the fast chemistry will generally have evolved within this timeframe (as shown in Fig. 1, enhanced background values occur off the Californian coast in May within 3 h).

4 Implementation and results

In most CTMs, the ship emissions are instantly diluted in the grid cell, thereby neglecting the non-linear chemistry in the early stages of the exhaust plume. In our approach, we use the LUTs calculated by PARANOX, containing the fraction of NO_x remaining and integrated NOPE, to account for the effects of plume dispersion and non-linear chemistry, by releasing reduced NO_x emissions and net O_3 produced and HNO3 into the large-scale global model.

ACPD
11, 17789–17823, 2011

4.1 GEOS-Chem

The chemistry transport model used in this study is GEOS-Chem version v8-03-02 (http://acmg.seas.harvard.edu/geos/) (Bey et al., 2001). We use GEOS-5 assimilated meteorological observations for the NASA Global Modeling and Assimilation Office (GMAO) to drive GEOS-Chem. The model has been run for tropospheric ozone-NOx-VOC-aerosol chemistry on a resolution of $2^{\circ} \times 2.5^{\circ}$, using a vertical grid containing 47 levels.

We perform a spin-up of one year (2004) and run the actual simulations for the year 2005. Since version v8-01-04, ship emitted NO_x molecules in GEOS-Chem are emitted as 1 molecule HNO_3 and 10 molecules O_3, based on the observations presented in Chen et al. (2005), to correct for the overproduction of O_3 by instantly diluting the NO_x emissions. We use the ICOADS global ship emissions inventory (Wang et al., 2008) and substitute this base inventory over Europe with the more detailed EMEP inventory (Vestreng et al., 2007). Neither inventory includes daily variation in the ship emissions, but the EMEP inventory includes seasonality.

4.1.1 Adaptations to GEOS-Chem

The sensitivity analysis showed that the fraction of NO_x remaining and integrated NOPE critically depend on 7 environmental parameters. We obtain these values from the GEOS-Chem simulation at the model time. Based on these values we calculate the fraction of NO_x remaining and the integrated NOPE (from linear interpolation between the closest reference values in the LUT). These calculated fraction of NO_x remaining and integrated NOPE are then used to release reduced NO_x emissions (and O_3 and HNO_3 produced), in order to appropriately simulate the effects of original emissions that took place 5 h earlier and have been subject to non-linear chemistry and dilution. In this approach we assume that the environmental parameters used in the LUT have not changed dramatically over the last 5 h. The changes in the photolysis values are modeled using the solar zenith angles which are calculated at each model time.

ACPD
11, 17789–17823, 2011

4.1.2 Additional simulations

For better understanding of the improved model and the effect of ship emissions, we adapted the GEOS-Chem model to also include instant dilution of the ship emitted NO_x molecules, and we adapted the standard model to include no ship emissions at all. The instant diluting model reflects how other global CTMs usually treat ship NO_x emissions, while comparison with the model with no ship emissions at all gives an indication of the effect of ship emissions on global atmospheric chemistry. We call the original model (v8-03-02, which releases every ship NO_x molecule as 1 molecule HNO_3 and 10 molecules O_3) the standard model.

4.2 Observations

In order to test our adaptations and extensions to the model we compare model simulations with measurements from dedicated campaigns, performed over the Pacific and Atlantic Ocean. We used data from the Pacific Exploratory Mission-West-A (PEM-West A) (Hoell et al., 1996) the Pacific Exploratory Mission-West-B (PEM-West B) (Hoell et al., 1997) and North Atlantic Regional Experiment (NARE) campaigns. PEM-West A was conducted over the North Pacific from 16 September till 21 October 1991, during a period of minimum outflow from Asia. PEM-West B was conducted from 7 February till 14 March 1994, during a period of enhanced outflow from Asia. NARE was conducted over the North Atlantic during September 1997 (Ryerson et al., 1999).

From the PEM-West A and PEM-West B measurement campaigns, we used the NO and O_3 measurements which were performed onboard a DC-8 aircraft. During PEM-West A and PEM-West B, NO was recorded using the chemiluminescence technique (Kondo et al., 1996).

We regridded observations for each $2^\circ \times 2.5^\circ$ grid cell, using the median of the observations to suppress influence from outliers. In contrast with the in-plume measurements reported by Chen et al. (2005), the PEM-West A and PEM-West B measurements used here represent the marine background concentrations (influenced by ship

ACPD
11, 17789–17823, 2011

emissions). Outliers in the PEM-West A and PEM-West B measurements could represent in-plume measurements and not the background concentrations.

For PEM-West A and PEM-West B, we limited the comparison with GEOS-Chem to grid boxes having observational data and being east of 145° E. This presumably reduces the influence of outflow from anthropogenic sources in Asia. For NARE we limited the comparisons to a latitude and longitude range of 37–50° N and 35–50° W, following Kasibhatla et al. (2000). This is also done to avoid the most intense continental outflow periods during this campaign. For all comparisons we compare average concentrations in the bottom 8 model levels (0 till 1.2 km) to the aircraft measurements below 1.2 km.

4.3 Comparison with observations

Figure 4 shows Box & Whisker plots of simulated and observed NO_x concentrations in the marine boundary layer for the PEM-West B, PEM-West A and NARE campaigns. The figure shows that NO_x concentrations simulated with the our LUT approach are in between the values simulated with the instant dilution and no ship emissions model for all campaigns. For PEM-West B, our new approach simulated NO_x concentrations are closest to observations. It is obvious that the standard model and model with no ship emissions simulate too little NO_x, and the instant diluting model strongly overestimates the amount of NO_x. Temporal mismatches are likely to contribute to the differences between simulated and observed values. It is obvious that over both oceans, the standard model simulates too little NO_x, and that instant diluting model always simulates too much NO_x.

Figure 5 shows a comparison of simulated and observed O_3 concentrations in the marine boundary layer for the PEM-West A and PEM-West B campaign. O_3 observations for the NARE campaign were not available in Kasibhatla et al. (2000), and we did not include simulations for this campaign. For both PEM-West A and PEM-West B, the standard model and the instant diluting model simulate the highest O_3 concentrations. For spring conditions (PEM-West B), the standard model simulates the

ACPD
11, 17789–17823, 2011

highest O_3 concentrations, as a consequence of its continuous O_3 production, also during darkness. The simulation without any ship emissions produces the smallest O_3 concentrations, and the difference of 1 ppbv with our new approach suggests that the overall effect of ships on springtime O_3 over the North Pacific is only small.

Both comparisons show that our new approach reduces NO_x and O_3 concentrations compared to the instant diluting approach, and simulates concentrations that are in better agreement with observations.

4.4 Comparison different GEOS-Chem simulations

Figure 6 shows the differences between the monthly mean (24 h mean) global NO_x and O_3 concentrations for January 2005 for the new LUT approach simulations and the instant diluting model simulations, for the lowest model layer (0–0.12 km).

Simulations using the new approach show NO_x concentrations that are lower by 0.1–0.2 ppbv (50 %) than the instant diluting simulation above ship track areas over the oceans, reflecting the in-plume NO_x destruction that is neglected in the instant diluting model. Above continental polluted areas (where chemistry is identical between the new approach and instant diluting), the new approach simulation leads to higher NO_x concentrations (by ~0.1 ppbv), but the relative differences over these polluted areas are negligible. The relative difference plot (Fig. 6, bottom right panel) confirms that the new approach simulation shows up to 60 % less NO_x in areas with frequently traveled ship tracks. On average NO_x concentrations in the new approach simulation are 44 % lower than in the instant diluting simulation over a latitude and longitude range of 20–40° W and 40–50° N in the North Atlantic in January 2005.

Figure 7 shows the difference plots in the monthly mean global NO_x concentrations for July 2005. In July the new approach simulates lower NO_x concentrations over the oceans (about 60 % less than the instant diluting simulation in ship tracks). NO_x concentrations in the new approach simulation are on average 60 % lower than in the instant diluting simulation in the 20–40° W and 40–50° N box in the North Atlantic.

ACPD
11, 17789–17823, 2011

Figure 8 shows the differences in the monthly mean global O_3 concentrations for January and July 2005. In January, the new approach simulates less O_3 (about 1 to 1.5 ppbv) over the oceans compared to the instantly diluting model, and 0.5 to 1 ppbv (2–4 %) less O_3 over large regions of the Northern Hemisphere. Over coastal waters in western Europe, our new approach simulates 0.5 to 1 ppbv lower O_3 concentrations. For comparison, Huszar et al. (2010) finds O_3 concentrations lower by 0.4 to 0.7 ppbv over these areas during winter.

In July, as a result of lower NO_x concentrations, the new approach simulation shows lower O_3 concentrations (up to 5 ppbv) over the oceans. Relative differences decrease over strongly polluted areas (e.g. North Sea or coastal China). In July the new approach simulates 25 % lower NO_x concentrations in the North Sea, and only 3 % lower O_3 concentrations.

Figure 9 shows the differences in the monthly mean global NO_x and O_3 concentrations for July 2005. The new approach simulation shows higher NO_x concentrations than the no ship emissions simulation. NO_x concentrations in the new approach simulation are on average 7× higher (44 pptv) over the averaged region in the North Atlantic in July. Over the averaged region in the North Atlantic, ships contribute 4 ppbv (15 %) to summertime O_3 concentrations.

5 Conclusions

We presented a computationally efficient approach to take the non-linear chemical effects that occur during the dispersion of NO_x emitted by ships into account in coarse-gridded global 3-D chemistry transport models (CTMs). Our approach uses a plume-in-grid treatment of ship emissions, with simulations from a plume dispersion model that takes the effects of non-linear chemistry fully into account. In addition to reduced NO_x emissions, the secondary compounds O_3 and HNO_3, produced in the 5 h after emission, are released into the global model.

ACPD
11, 17789–17823, 2011

To simulate the in-plume effects, we use the 10-ring Gaussian plume dispersion PARANOX model with state-of-science chemical rate constants, updated emissions, photolysis constants, and dispersion parameters relevant for the marine boundary layer. We evaluated simulations by the PARANOX model against in situ aircraft observations of NO_x, O_3, and (inferred) OH concentrations within fresh ship plumes off the coast of California in May 2002, and find that PARANOX captures the essence of ship-plume chemistry.

A sensitivity analysis showed that plume-in-grid simulations depend critically on ambient temperature, ozone concentration, NO_x concentration, the solar zenith at the time of initial, and actual (5 h after) release, and photolysis rate constants for NO_2 and $O(^1D)$.

Our approach couples the plume dispersion model PARANOX to a global model, here the 3-D GEOS-Chem CTM, in a computationally efficient manner. For every grid cell with non-zero ship NO_x emissions, the global model chemical simulations provide the relevant environmental parameters, and we subsequently retrieve the matching fraction of NO_x remaining and secondary species from the look-up table. We then use the fraction of NO_x remaining to reduce the original ship NO_x emissions, and release the O_3 and HNO_3 produced during plume dispersion into the GEOS-Chem background state.

We adapted the GEOS-Chem model to also include options to simulate ship emissions with the widely used "instant dilution" approach, and without any ship emissions at all. Together with the standard model (that emits ship NO_x molecule as 1 HNO_3 and 10 O_3 molecules), and the improved model with the plume-in-grid approach, this provides an ensemble that allowed for a comprehensive intercomparison, as well as an evaluation against observations from (historical) aircraft campaigns over the Pacific Ocean (PEM-West A and PEM-West B) and over the North Atlantic (NARE).

We found that our improved version of GEOS-Chem simulates up to 0.1 ppbv more NO_x over the North Atlantic in July compared to simulations without ship NO_x emissions, indicating that ships contribute up to 90 % to total nitrogen oxide concentrations

ACPD
11, 17789–17823, 2011

over this region. Compared to simulations using the instant dilution approach, our NO_x concentrations are 0.05–0.15 ppbv lower, indicating that models using instant dilution overestimate NO_x over the North Atlantic by approximately 50 %. These conclusions are supported by a comparison of simulated and observed NO_x concentrations in the lower marine atmosphere (PEM-West B). We found that our improved model matches the observed NO_x concentrations best, whereas the instant diluting model overestimates NO_x by a factor of 2, and the models without ship emissions underestimate NO_x by a factor of 0.7.

Our improved model simulates up to 4 ppbv more O_3 over the North Atlantic during summer than the model without ship emissions. Ozone concentrations simulated with the improved model are 3–5 ppbv (10–25 %) lower than with the instant dilution approach over the Atlantic Ocean, clearly indicating that instant dilution not only overestimates nitrogen oxides, but also ozone. Over the strongly polluted North Sea, the improved simulations show smaller ozone reductions of 1–2 ppbv (<5 %) compared to the instant diluting approach, suggesting that accounting for non-linear in-plume chemistry is most relevant for pristine, unpolluted areas.

Acknowledgements. This research was funded by the Netherlands Organisation for Scientific Research, NWO Vidi grant 864.09.001. Work at Harvard was funded by the NASA Atmospheric Composition Modeling and Analysis Program.

References

Bey, I., Jacob, D. J., Yantosca, R. M., Logan, J. A., Field, B. D., Fiore, A. M., Li, Q., Liu, H. Y., Mickley, L. J., and Schultz, M. G.: Global modeling of tropospheric chemistry with assimilated meteorology: Model description and evaluation, J. Geophys. Res., 106, 23073–23095, 2001. 17792, 17802

Charlton-Perez, C. L., Evans, M. J., Marsham, J. H., and Esler, J. G.: The impact of resolution on ship plume simulations with NO_x chemistry, Atmos. Chem. Phys., 9, 7505–7518, doi:10.5194/acp-9-7505-2009, 2009. 17792, 17814

ACPD

11, 17789–17823, 2011

Chen, G., Huey, L. G., Trainer, M., Nicks, D., Corbett, J., Ryerson, T., Parrish, D., Nueman, J. A., Nowak, J., Tanner, D., Holloway, J., Brock, C., Crawford, J., Olson, J. R., Sullivan, A., Weber, R., Schauffler, S., Donnelly, S., Atlas, E., Roberts, J., Flocke, F., Hübler, G., and Fehsenfeld, F.: An investigation of the chemistry of ship emissions plumes during ITCT 2002, J. Geophys. Res., 110, D10S90, doi:10.1029/2004JD005236, 2005. 17792, 17794, 17795, 17802, 17803, 17813, 17814, 17815

Corbett, J. J., Fischbeck, P. S., and Pandis, S. N.: Global nitrogen and sulfur inventories for oceangoing ships, J. Geophys. Res., 104, 3457–3470, 1999. 17791

Corbett, J. J., Winebrake, J. J., Green, E. H., Kasibhatla, P., Eyring, V., and Lauer, A.: Mortality from Ship Emissions: A Global Assessment, Environ. Sci. Technol., 41, 8512–8518, 2007. 17791

Davis, D. D., Grodzinsky, G., Kasibhatla, P., Crawford, J., Chen, G., Liu, S., Bandy, A., Thornton, D., Guan, H., and Sandholm, S.: Impact of Ship Emissions on Marine Boundary Layer NO_x and SO_2 Distributions over the Pacific Basin, Geophys. Res. Lett., 28, 235–238, 2001. 17791

DeMore, W. B., Sander, S. P., Golden, D. M., Hampson, R. F., Kurylo, M. J., Howard, C. J., Ravishankara, A. R., and Kolb, C. E.: Chemical kinetics and photochemical data for use in stratospheric modeling, JPL-Publ., 97-4, 1997. 17794

Duncan, B. N., West, J. J., Yoshida, Y., Fiore, A. M., and Ziemke, J. R.: The influence of European pollution on ozone in the Near East and northern Africa, Atmos. Chem. Phys., 8, 2267–2283, doi:10.5194/acp-8-2267-2008, 2008. 17792

Evans, M. J. and Jacob, D. J.: Impact of new laboratory studies of N_2O_5 hydrolysis on global model budgets of tropospheric nitrogen oxides, ozone and OH, Geophys. Res. Lett., 32, L09813, doi:10.1029/2005GL022469, 2005. 17794

Eyring, V., Köhler, H. W., van Aardenne, J., and Lauer, A.: Emissions from international shipping: 1. The last 50 years, J. Geophys. Res., 110, D17305, doi:10.1029/2004JD005619, 2005. 17791, 17814

Eyring, V., Isaksen, I. S. A., Berntsen, T., Collins, W. J., Corbett, J. J., Endresen, O., Grainger, R. G., Moldanova, J., Schlager, H., and Stevenson, D. S.: Transport impacts on atmosphere and climate: Shipping, Atmos. Environ., 44, 4735–4771, 2010. 17790, 17791

Franke, K., Eyring, V., Sander, R., Hendricks, J., Lauer, A., and Sausen, R.: Toward effective emissions of ships in global models, Meteorol. Z., 17, 117–129, 2008. 17792, 17795, 17801, 17814

Hanna, S. R., Schulman, L. L., Paine, R. J., and Pleim, J. E.: Development and Evaluation of

ACPD
11, 17789–17823, 2011

the Offshore and Coastal Dispersion Model, J. Air Pollut. Control Assoc., 35, 1039–1047, 1985. 17795
Hoell, J. M., Davis, D. D., Lui, S. C., Newell, R., Shipham, M., Akimoto, H., McNeal, R. J., Bendura, R. J., and Drewry, J. W.: Pacific Exploratory Mission-West A (PEM-West A): September–October 1991, J. Geophys. Res., 101, 1641–1653, 1996. 17803
Hoell, J. M., Davis, D. D., Lui, S. C., Newell, R. E., Akimoto, H., McNeal, R. J., and Bendura, R. J.: Pacific Exploratory Mission-West Phase B: Feburary–March 1994, J. Geophys. Res., 102, 28223–28239, 1997. 17803
Huszar, P., Cariolle, D., Paoli, R., Halenka, T., Belda, M., Schlager, H., Miksovsky, J., and Pisoft, P.: Modeling the regional impact of ship emissions on NO_x and ozone levels over the Eastern Atlantic and Western Europe using ship plume parameterization, Atmos. Chem. Phys., 10, 6645–6660, doi:10.5194/acp-10-6645-2010, 2010. 17793, 17806
IPCC 2007, Climate Change 2007: Impacts, Adaptation and Vulnerability. Contribution of Working Group II to the Fourth Assessment Report of the Intergovernmental Panel on Climate Change, edited by: Parry, M. L., Canziani, O. F., Palutikof, J. P., van der Linden, P. J., and Hanson, C. E., Cambridge University Press, Cambridge, UK, 976 pp., 2007. 17791
Kasibhatla, P., II, H. L., Moxim, W. J., Pandis, S. N., Corbett, J. J., Peterson, M. C., Honrath, R. E., Frost, G. J., Knapp, K., Parrish, D. D., and Ryerson, T. B.: Do emissions from ships have a significant impact on concentrations of nitrogen oxides in the marine boundary layer?, Geophys. Res. Lett., 27, 2229–2232, 2000. 17791, 17804, 17818
Kim, H. S., Song, C. H., Park, R. S., Huey, G., and Ryu, J. Y.: Investigation of ship-plume chemistry using a newly-developed photochemical/dynamic ship-plume model, Atmos. Chem. Phys., 9, 7531–7550, doi:10.5194/acp-9-7531-2009, 2009. 17795, 17813, 17814
Kondo, Y., Ziereis, H., Koike, M., Kawakami, S., Gregory, G. L., Sachse, G. W., Singh, H. B., Davis, D. D., and Merril, J. T.: Reactive nitrogen over the Pacific Ocean during PEM-West A, J. Geophys. Res., 101, 1809–1828, 1996. 17803
Lawrence, M. G. and Crutzen, P. J.: Influence of NO_x emissions from ships on tropospheric photochemistry and climate, Nature, 402, 167–170, 1999. 17791
Marmer, E., Dentener, F., Aardenne, J. v., Cavalli, F., Vignati, E., Velchev, K., Hjorth, J., Boersma, F., Vinken, G., Mihalopoulos, N., and Raes, F.: What can we learn about ship emission inventories from measurements of air pollutants over the Mediterranean Sea?, Atmos. Chem. Phys., 9, 6815–6831, doi:10.5194/acp-9-6815-2009, 2009. 17791
Meijer, E. W.: Modelling the impact of subsonic aviation on the composition of the atmosphere,

ACPD
11, 17789–17823, 2011

Ph.D. thesis, Eindhoven University of Technology, 2001. 17793
Meijer, E. W., van Velthoven, P. F. K., Wauben, W. M. F., Beck, J. P., and Velders, G. J. M.: The effects of the conversion of nitrogen oxides in aircraft exhaust plumes in global models, Geophys. Res. Lett., 24, 3013–3016, 1997. 17793
Ryerson, T. B., Huey, L. G., Knapp, K., Neuman, J. A., Parrish, D. D., Sueper, D. T., and Fehsenfeld, F. C.: Design and initial characterization of an inlet for gas-phase NO_y measurements from aircraft, J. Geophys. Res., 104, 5483–5492, 1999. 17803
Schlager, H., Baumann, R., Lichtenstern, M., Petzold, A., Arnold, F., Speidel, M., Gurk, C., and Fischer, H.: Aircraft-based trace gas measurements in a primary European ship corridor, Proceedings of the International Conference on Transport, Atmosphere and Climate (TAC), Oxford, UK, 83–88, 2008. 17801, 17814
Sillman, S., Logan, J. A., and Wofsy, S. C.: A regional scale model for ozone in the United States with subgrid representation of urban and power plant plumes, J. Geophys. Res., 95, 5731–5748, 1990. 17793
Song, C. H., Chen, G., Hanna, S. R., Crawford, J., and Davis, D. D.: Dispersion and chemical evolution of ship plumes in the marine boundary layer: Investigation of $O_3/NO_y/HO_x$ chemistry, J. Geophys. Res., 108, 4143, doi:10.1029/2002JD002216, 2003. 17792, 17795, 17814
Song, C. H., Kim, H. S., von Glasow, R., Brimblecombe, P., Kim, J., Park, R. J., Woo, J. H., and Kim, Y. H.: Source identification and budget analysis on elevated levels of formaldehyde within the ship plumes: a ship-plume photochemical/dynamic model analysis, Atmos. Chem. Phys., 10, 11969–11985, doi:10.5194/acp-10-11969-2010, 2010. 17795
Vestreng, V., Mareckova, K., Kakareka, S., Malchykhina, A., and Kukharchyk, T.: Inventory Review 2007; Emission Data reported to LRTAP Convention and NEC Directive, MSC-W Technical Report 1/07, Tech. rep., The Norwegian Meteorological Institute, Oslo, Norway, 2007. 17802
Vinken, G. C. M.: Accounting for non-linear chemistry of shipping plumes in a Global Chemistry Transport Model, M.Sc.-Thesis, R-1772-A, Eindhoven University of Technology, 2010. 17793
von Glasow, R., Lawrence, M. G., Sander, R., and Crutzen, P. J.: Modeling the chemical effects of ship exhaust in the cloud-free marine boundary layer, Atmos. Chem. Phys., 3, 233–250, doi:10.5194/acp-3-233-2003, 2003. 17792, 17814
Wang, C., Corbett, J. J., and Firestone, J.: Improving Spatial Representation of Global Ship Emissions Inventories, Environ. Sci. Technol., 42, 193–199, 2008. 17791, 17802

ACPD
11, 17789–17823, 2011

Table 1. Most critical $O_3/NO_y/HO_x$ reactions in PARANOX for both day and nighttime. We use *R*H as simplified notation for Volatile Organic Compounds (VOCs) (*R* represents an organic group).

(R1)*	$O_3 + h\nu + H_2O \rightarrow x_1\,OH + x_2\,O_3 + O_2$
(R2)	$NO_2 + OH + M \rightarrow HNO_3 + M$
(R3)	$O_3 + NO \rightarrow NO_2 + O_2$
(R4)	$NO + HO_2 \rightarrow NO_2 + OH$
(R5)	$NO_2 + h\nu \xrightarrow{O_2} NO + O_3$
(R6)	$O_3 + NO_2 \rightarrow NO_3 + O_2$
(R7)	$NO_2 + NO_3 + M \rightarrow N_2O_5 + M$
(R8)	$CH_4 + OH \xrightarrow{O_2} CH_3O_2 + H_2O$
(R9)	$CH_3O_2 + NO \xrightarrow{O_2} HCHO + HO_2 + NO_2$
(R10)	$CO + OH \xrightarrow{O_2} HO_2 + CO_2$
(R11)	$NO_3 + h\nu \xrightarrow{O_2} NO_2 + O_3$
(R12)	$N_2O_5 + H_2O \xrightarrow{aer.} 2HNO_3$
(R13)	$RH + OH \xrightarrow{O_2} RO_2 + H_2O$
(R14)	$RO_2 + NO \rightarrow RO + NO_2$

* This reaction is a net reaction of the loss of O_3 by photolysis to $O(^1D)$, followed by three possible reactions. The $O(^1D)$ can react with H_2O forming 2 OH molecules, the $O(^1D)$ can react with N_2 forming $O(^3P)$ and N_2 or the $O(^1D)$ can react with O_2 forming $O(^3P)$ and O_2. From these last two possibilities, the $O(^3P)$ can react with O_2 producing O_3. In Eeaction (R1) x_1 and x_2 are stochiometric coefficients, quantifying the relationship of reactants and products in this net reaction ($x_1 + x_2 = 1$). These stochiometric coefficients are calculated in PARANOX and depend on temperature, air density and H_2O concentrations.

ACPD
11, 17789–17823, 2011

Table 2. Ambient concentrations used in the PARANOX simulation for comparison with ITCT 2k2 observations (Chen et al., 2005)*.

Species	O_3	NO_x	HNO_3	CO	SO_2	PAN	CH_3CHO	CH_3OH
Ambient Concentration (ppbv)	40.5	0.150	0.005	130	0.4	0.16	0.1	0.25

* During the measurements the wind speed was between 9 and 11 $m\,s^{-1}$, in this comparison we set the wind speed to 10 $m\,s^{-1}$. The height of the marine boundary layer determined from aircraft measurements was 350 m. The ambient temperature was 290 K. We set the stability class to "moderately stable", following a recent study by Kim et al. (2009).

ACPD
11, 17789–17823, 2011

Table 3. Summary of NO_x ship emissions strengths currently used in literature.

Study	NO_x emission strength ($g\,s^{-1}$)
Charlton-Perez et al. (2009)	33
Franke et al. (2008)	145[a]
Schlager et al. (2008)	184[a]
Kim et al. (2009)	6.25[b]
Chen et al. (2005)	13.4
Song et al. (2003)	4–20
von Glasow et al. (2003)	19.1
Eyring et al. (2005)	9.31[c]
This study	20

[a] The emission strengths reported by Franke et al. (2008) and Schlager et al. (2008) hold for "fairly large container ships".
[b] Based on Chen et al. (2005).
[c] Calculated using annual emissions of cargo ships.

ACPD
11, 17789–17823, 2011

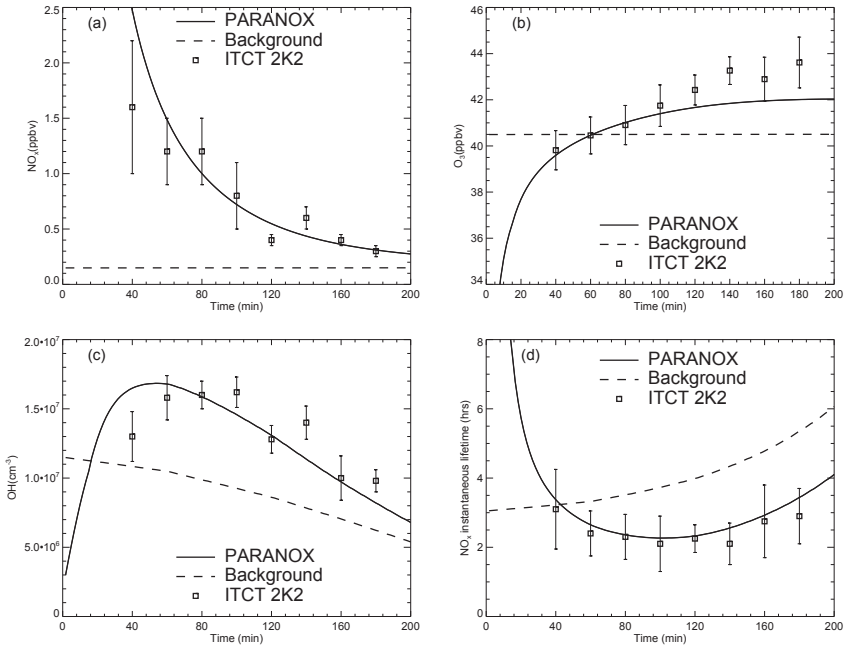

Fig. 1. Observed and simulated concentrations averaged over the cross-section of a ship plume released at 12.00 hours local time as function of time since release for the species: **(a)** NO_x; **(b)** O_3; **(c)** OH and **(d)** the NO_x instantaneous lifetime as function of time. The solid line indicates the PARANOX simulation with ambient concentrations given in Table 2. The dashed line represents the background concentration and the squares represent the observations taken during the ITCT 2K2 aircraft campaign on 8 May 2002, with the bars indicating measurement errors. The OH concentrations in **(c)** were inferred from H_2SO_4 measurements (Chen et al., 2005). The NO_x instantaneous lifetime was calculated as the NO_x concentration divided by the production rate of HNO_3 at any point in time.

ACPD
11, 17789–17823, 2011

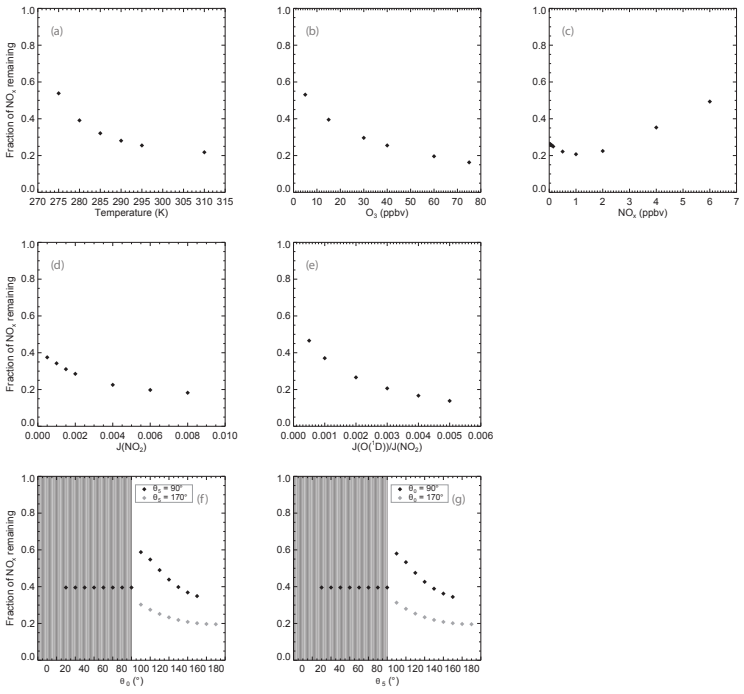

Fig. 2. PARANOX simulations of the fraction of NO_x remaining after 5 hours for a plume released at 12.00 hours local time as a function of: **(a)** Temperature; **(b)** ambient O_3 concentration; **(c)** ambient NO_x concentration; **(d)** $J(NO_2)$; **(e)** $\frac{J(NO_2)}{J(O(^1D))}$; **(f)** θ_0 and **(g)** θ_5. The simulation in panel **(f)** and **(g)** were not released at 12:00 h, but for different initial solar zenith angles, corresponding to a variety of release hours at different latitudes. The shaded areas in panel **(f)** and **(g)** corresponds to simulations during darkness. A NO_x emissions strength of 20 g s$^-$1 has been used. Ambient meteorological conditions are a neutral stability class, wind velocity of 8 m s^{-1}, temperature of 295 K and marine boundary layer height of 400 m. Ambient concentrations for O_3 and NO_x were set to 40 ppbv and 100 pptv, respectively.

ACPD
11, 17789–17823, 2011

Ship plumes in the GEOS-Chem global chemistry transport model

G. C. M. Vinken et al.

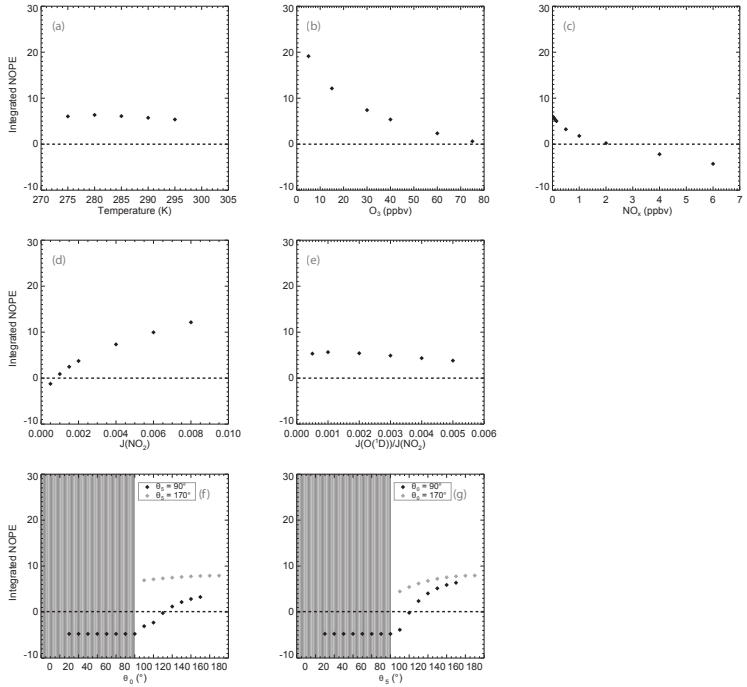

Fig. 3. PARANOX simulations of the integrated net ozone production efficiency (NOPE) after 5 h for a plume released at 12:00 h local time as a function of: **(a)** temperature; **(b)** ambient O_3 concentration; **(c)** ambient NO_x concentration; **(d)** $J(NO_2)$; **(e)** $\frac{J(NO_2)}{J(O(^1D))}$; **(f)** θ_0 and **(g)** θ_5. The shaded area in panel **(f)** and **(g)** corresponds to simulations during darkness. Ambient meteorological conditions and concentrations as in Fig. 2.

ACPD
11, 17789–17823, 2011

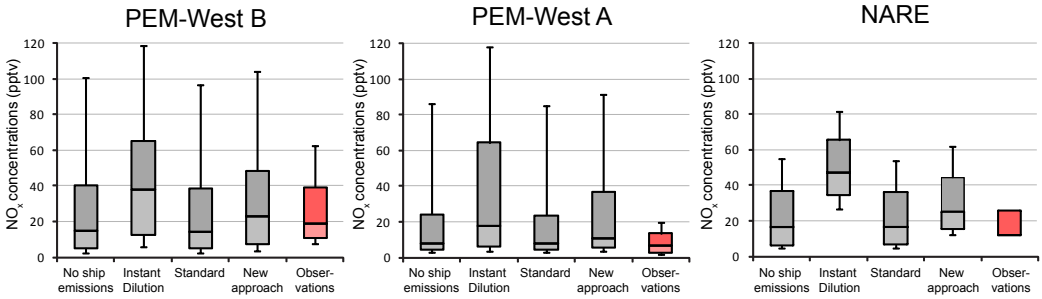

Fig. 4. Box & Whisker plot of simulated and observed median NO_x concentrations (in pptv) for the PEM-West B campaign (left), the PEM-West A campaign (middle) and the NARE campaign (right). The box shows the data between the upper and lower quartiles (25th and 75th percentile), with the median represented by a horizontal line; whiskers go out to the 5th and 95th percentile of the data. PEM-West B measurements were taken during 7 February till 14 March 1994, PEM-West A measurements were taken during 16 September till 21 October 1991 and NARE measurements were taken during September 1994. Simulations were performed for the year 2005. The PEM-West A and PEM-West B data was obtained from the Atmospheric Chemistry Division, National Center for Atmospheric Research, University Corporation for Atmospheric Research (available at http://cdp.ucar.edu/). For the NARE campaign we use statistics reported in Kasibhatla et al. (2000). We converted all NO measurements into NO_x concentrations using the $\frac{NO}{NO_x}$ ratio derived from GEOS-Chem simulations.

ACPD
11, 17789–17823, 2011

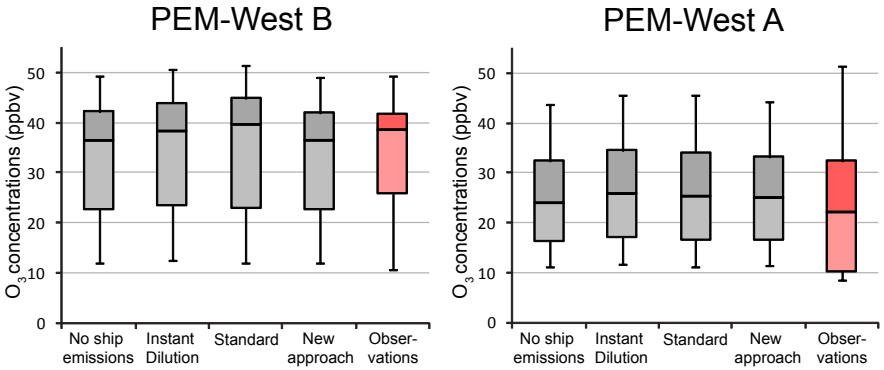

Fig. 5. Box & Whisker plot of simulated and observed median O_3 concentrations (in ppbv) for the PEM-West B campaign (left) and the PEM-West A campaign (right).

ACPD
11, 17789–17823, 2011

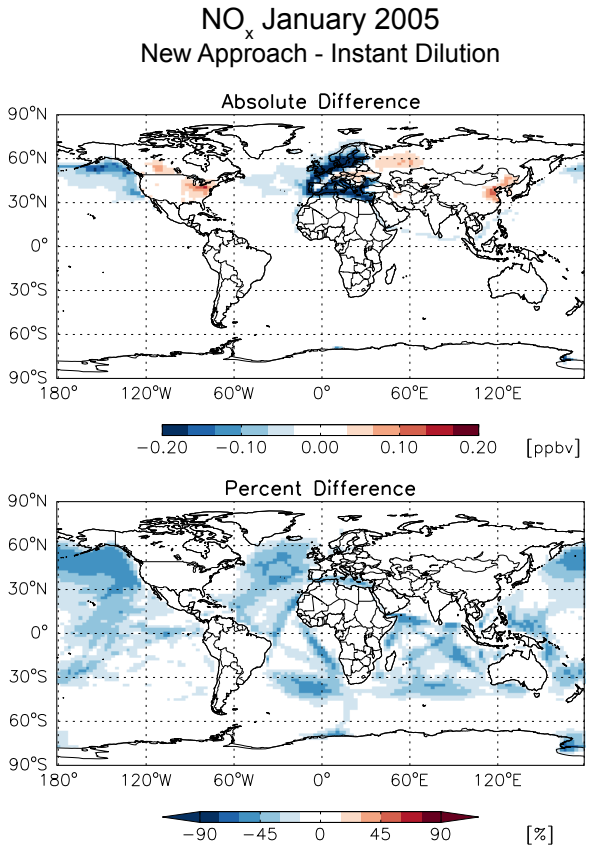

Fig. 6. Difference plots between monthly mean global NO_x concentrations simulated with GEOS-Chem for January 2005 for the instant diluting model and the new LUT approach model simulations, for the lowest model layer (0–0.12 km).

ACPD
11, 17789–17823, 2011

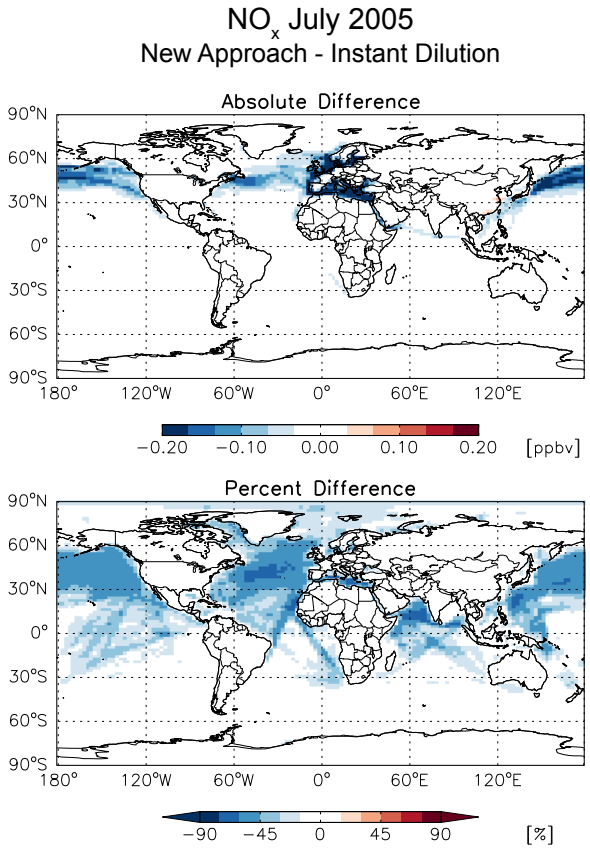

Fig. 7. Difference plots between monthly mean global NO_x concentrations simulated with GEOS-Chem for July 2005 for the instant diluting model and the new LUT approach model simulations, for the lowest model layer (0–0.12 km).

ACPD
11, 17789–17823, 2011

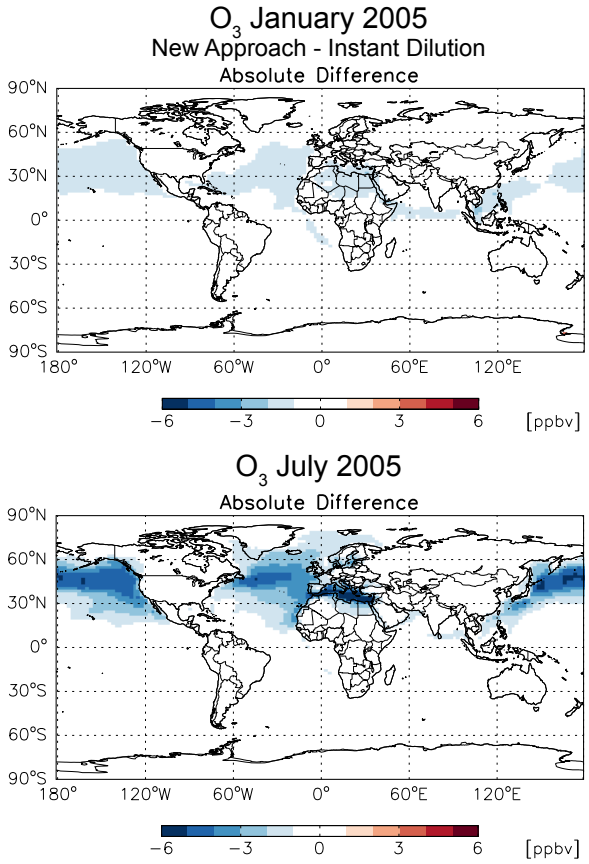

Fig. 8. Absolute difference plots between monthly mean global O_3 concentrations simulated with GEOS-Chem for January and July 2005 for the instant diluting model and the new LUT approach model simulations, for the lowest model layer (0–0.12 km).

ACPD
11, 17789–17823, 2011

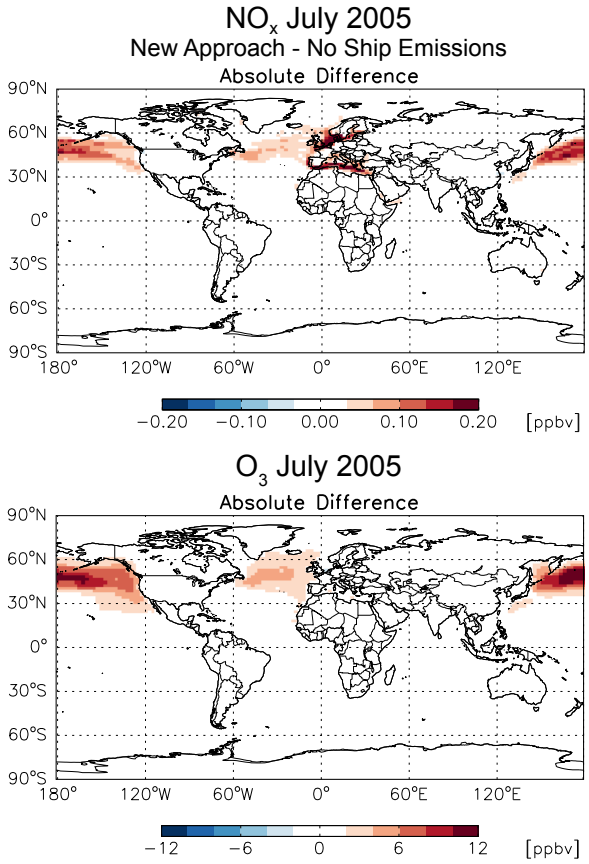

Fig. 9. Absolute difference plots between monthly mean global NO_x and O_3 concentrations simulated with GEOS-Chem for July 2005 for the no ship emissions model and the new LUT approach model simulations, for the lowest model layer (0–0.12 km).

ACPD
11, 17789–17823, 2011